Journal of Colloid and Interface Science 565 (2020) 119–130

Contents lists available at ScienceDirect

Journal of Colloid and Interface Science

journal homepage: www.elsevier.com/locate/jcis

Pluronic F127 thermosensitive injectable smart hydrogels for controlled drug delivery system development

Bana Shriky [a,*], Adrian Kelly [a], Mohammad Isreb [b], Maksims Babenko [a], Najet Mahmoudi [c], Sarah Rogers [c], Olga Shebanova [d], Tim Snow [d], Tim Gough [a,*]

[a] Faculty of Engineering and Informatics, Faculty of Life Sciences-University of Bradford, UK
[b] Faculty of Life Sciences-University of Bradford, UK
[c] ISIS, STFC, Rutherford Appleton Laboratory, Didcot, UK
[d] Diamond Light Source, STFC, Rutherford Appleton Laboratory, Didcot, UK

GRAPHICAL ABSTRACT

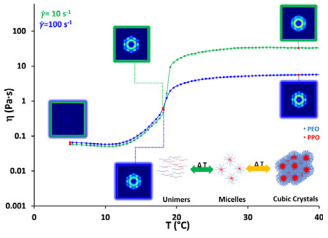

ARTICLE INFO

Article history:
Received 27 August 2019
Revised 20 December 2019
Accepted 21 December 2019
Available online 23 December 2019

Keywords:
Thermosensitive
Gel
Thermal properties
Rheological properties
SAXS
SANS
Drug release
Pluronic
Colloidal crystals
Drug delivery systems
Injectables

ABSTRACT

Understanding structure-property relationships is critical for the development of new drug delivery systems. This study investigates the properties of Pluronic smart hydrogel formulations for future use as injectable controlled drug carriers. The smart hydrogels promise to enhance patient compliance, decrease side effects and reduce dose and frequency. Pharmaceutically, these systems are attractive due to their unique sol-gel phase transition in the body, biocompatibility, safety and injectability as solutions before transforming into gel matrices at body temperature. We quantify the structural changes of F127 systems under controlled temperature after flow, as experienced during real bodily injection. Empirical formulae combining the coupled thermal and shear dependency are produced to aid future application of these systems. Induced structural transitions measured in-situ by small angle x-ray and neutron scattering reveal mixed oriented structures that can be exploited to tailor the drug release profile.

1. Introduction

Advances in biomedical and material sciences have led to a rapid intensification in development and exploration the use of selective Drug Delivery Systems (DDSs) that offer improved control of administered drug release, providing protection for the

* Corresponding authors.
E-mail addresses: B.shriky1@bradford.ac.uk (B. Shriky), A.L.Kelly@bradford.ac.uk (A. Kelly), M.Isreb1@bradford.ac.uk (M. Isreb), M.Babenko1@bradford.ac.uk (M. Babenko), najet.mahmoudi@stfc.ac.uk (N. Mahmoudi), sarah.rogers@stfc.ac.uk (S. Rogers), olga.shebanova@diamond.ac.uk (O. Shebanova), tim.snow@diamond.ac.uk (T. Snow), T.Gough@bradford.ac.uk (T. Gough).

https://doi.org/10.1016/j.jcis.2019.12.096
0021-9797/

delivered therapeutic agent against degradation and safety from accidental release. These DDSs offer reduced side effects and enhanced efficacy compared to conventional dosage forms [1,2]. Global revenue for DDSs was estimated to be $181.9 billion in 2013 and is expected to grow at a Compound Annual Growth Rate of around 3.2% to reach up to $212.8 billion by 2019 [3,4].

These DDSs are manufactured in the form of emulsions, liposomes, microspheres and colloidal gels. They are self-sustaining systems working as drug reservoirs or carriers optimised depending on application requirements and releasing the bioactive molecules when triggered by specific endogenous or exogenous stimuli, offering spatial and temporal control over the release process. Examples which have entered their clinical phases include; Doxil, thermoDox and Nanotherm [5,6].

Injectable smart gel systems spontaneously form a network as a response to specific stimuli, and are classified according to their particular triggers e.g. pH, UV photopolymerization, stereocomplexation, charge interaction, ultrasound, electromagnetic radiation and temperature [7–12]. These smart systems have tunable porosity allowing controlled loading and release from the gel network, and work as depots injected into the body as impregnated solutions before undergoing a first order transition producing flexible soft hydrogel matrices in-situ at the physiological temperature. They exhibit good adhesion and low interfacial tension thus resembling a living cell's extracellular matrices, and body tissues, hence reducing the possibility of immune responses.

Gel design should focus on the salient features desired for the application determined by material crosslinking, biodegradability and biochemical stability [7,8]. These factors inevitably influence the physical, structural and mechanical behaviours of the gel matrix during and after injection. The mechanical behaviour reflects the hydrogel's structure-property relationship and conveys the structural transitions the DDS undergoes during administration by passing through different environments (temperature and shear), which can influence stability, drug deposition and release [9,10].

Amphiphilic block copolymers are among the most commonly used substrates for injectable drug delivery. The PEO-based non-ionic surfactants, Pluronics® (known alternatively as Poloxamers®), are composed of polyethylene oxide-polypropylene oxide-polyethylene oxide (PEO-PPO-PEO) triblock coploymers. Pluronics' attractiveness can be attributed to their safety, bioadhesiveness, stability and ability to form gels at low concentrations at body temperature. Gelation properties may be readily tuned using physical blends of Pluronics or other excipients [11–15].

Dilute solutions of block copolymers self-assemble to form micelles in 'good' solvents upon reaching a critical micellar temperature (CMT) as a result of PPO-block dehydration. These micelles have a relatively compact core and a heavily solvated corona. At sufficient concentrations, the triblock micelles associate above a critical gelation temperature (CGT) and order onto a lyotropic liquid crystalline (LLC) phase, a complex liquid phase with characteristics of both anisotropic crystalline solids and isotropic liquids. These micellar liquids can be described as colloidal dispersions of hard spheres which undergo a hard sphere crystallisation to form the gel structure above CGT [16–19]. The variety of mesophases reported for the same triblocks by different groups are largely attributed to polymerisation by-products, which affect the self-assembly leading to formation of different phases before and after polymer purification [20,21].

During drug administration, the polymeric matrices are subjected to shear that alters the spatial arrangement of the particles making up the colloidal crystal, leading to the macroscopic viscoelastic response recorded for this class of materials.

This study builds upon previous works on similar systems and provides a comprehensive dynamic study of an injectable polymeric delivery system of Pluronic F127® (Poloxamer 407®), by evaluating gelation, microscopic and macroscopic structural changes at equilibrium and non-equilibrium conditions in controlled environments as measured by rheology in conjunction with time-resolved SAXS and SANS.

2. Experimental methods

2.1. Sample preparation

Pluronic® F127 with molecular weight of 12600 g/mol was obtained from Sigma-Aldrich (St. Louis, MO) and used as received. Formulations were prepared according to the cold method by Schmolka [22]. F127 concentrations of 0.1–35% (w/w%) were prepared by dissolving the copolymer in deionized water (18 MΩ cm) or deuterium oxide (99.8%) at a temperature below 4 °C, and left to rest for at least 24 h before performing characterisation.

2.2. Differential scanning calorimetry (DSC)

A TA Discovery DSC connected to an RCS-90 cooling system (New Castle, USA) was used to study the thermal transition associated with micellisation. An average sample size of 15 mg was loaded into '*T*-zero' hermetic pans and scans were performed from −20 to 45 °C at a standard heating rate of 10 °C/min.

2.3. Rheometry

Rheological measurements were conducted on Anton-Paar Physica MCR 301 and 501 (Graz, Austria) rheometers using a CC27 (gap = 1.23 mm) Couette cylinder geometry with a solvent trap and a Peltier temperature controlled stage, allowing the application of fixed temperature and ramps ranging from 0 to 100 °C. Tests were performed in both rotational and oscillatory shear modes, where shear rates applied in rotational mode were from 10 to 1500 s^{-1}. Oscillation parameters of ω = 10 rad/*sec* with a strain of γ = 0.2% were applied, this falling within the linear viscoelastic region.

2.4. Small angle scattering

2.4.1. X-ray small angle scattering (SAXS)

Dynamic SAXS was performed using the I22 beamline at Diamond Light Source (Didcot, UK), with an x-ray wavelength of 0.88 Å and sample-to-detector distance (SDD) fixed at 1.9 m permitting measurements in the range $0.014 \leq q\ Å^{-1} \leq 0.524$, where $q = 4\pi\sin(\theta/2)/\lambda$, 2Θ is the scattering angle and λ is the wavelength. Data were collected from two experimental setups: (1) Constant shear with temperature ramps using a Linkam optical Shearing System CSS450 (Tadworth, UK) with modified x-ray transparent Polyimide (Kapton) windows and a gap of 500μm, (2) Injection of formulations from a 20 ml chilled syringe into an in-house designed Polyimide reservoir with a channel diameter of 3 mm mounted on an Aladdin remotely controlled syringe pump (World Precision Instruments, USA). During the experiments temperature control was maintained by a Lauda Eco-Re415 chiller (Konigshofen, Germany). Schematics of the experimental setups are provided in Figure SI 1.

2.4.2. Neutron small angle scattering (SANS)

Static SANS experiments were carried out at the ISIS Neutron and Muon source (Didcot, UK), where data were collected using the LOQ SANS beamline with an SDD of 4 m covering a range of $0.007 \leq q\ Å^{-1} \leq 1.5$. Quartz cuvettes with path lengths of 2 mm

were used for all measurements at two different temperatures of 5 and 37° C.

Dynamic SANS under steady shear conditions was performed on the SANS2D instrument using an Anton-Paar Physica MCR 501 rheometer with a customized quartz Couette cell and a temperature controller (TC-30) [23]. Rheo-SANS measurements were recorded with a quartz Couette geometry with a gap of 1 mm with the beam in the radial direction [24]. The formulation's properties were investigated under two shear rates (10 and 100 s^{-1}) and three characteristic temperatures.

3. Results and discussion

3.1. Static measurements

3.1.1. Thermal properties

The endothermic thermal transition limits of the formulations were investigated by calorimetry, allowing for the quantification of the self-assembly onset (T_{onset}), micellisation peak (T_{peak}) and endset (T_{endset}) temperatures. The effect of increased concentration on transitions is evident in the endothermic peaks' shift to lower temperatures as seen in Fig. 1-a, the recorded values being in close proximity to those reported in the literature [25,26]. The thermograms revealed a monotonic increase in peak enthalpy (ΔH) as a function of concentration. The trend shown in Fig. 1-b can be used to predict the process enthalpy per gram of F127 in the formulation using the linear function:

$$\Delta H = a(C_{F127}) + m \quad (1)$$

where a = 0.193 J/g, m = 0.43 J/g

The cooling ramps confirmed the transition reversibility and showed the same concentration dependency seen in the heating ramps - see Figure SI 2.

3.1.2. Morphological properties

Fig. 2-a shows the scattering profiles from the deuterated formulations at 5 °C. All concentrations exhibit a broad micellar shoulder around q = 0.1 $Å^{-1}$ which becomes better defined and shifts to higher q-values with increasing concentration, which, according to Prud'homme *et al.*, represents interparticle interactions in the system [27]. For 30% F127 a peak appeared at q = 0.036 $Å^{-1}$ indicating that a structural transition was commencing.

At 37 °C the systems exhibit more defined scattering profiles with better defined peaks that correspond to a paracrystal structure. The signal's strength was proportional to the polymer concentration as seen in Fig. 2-b. As concentration increases, the first peak (q*) shifts to higher q-values correlating to a decrease in the lattice spacing and therefore increased packing density. The structure was identified as face centered cubic (FCC) based on this peak's ratio to the first peak (q_n/q^*), in agreement to literature for unpurified F127 systems [28–30]. The arrows in Fig. 2-b represent the peaks

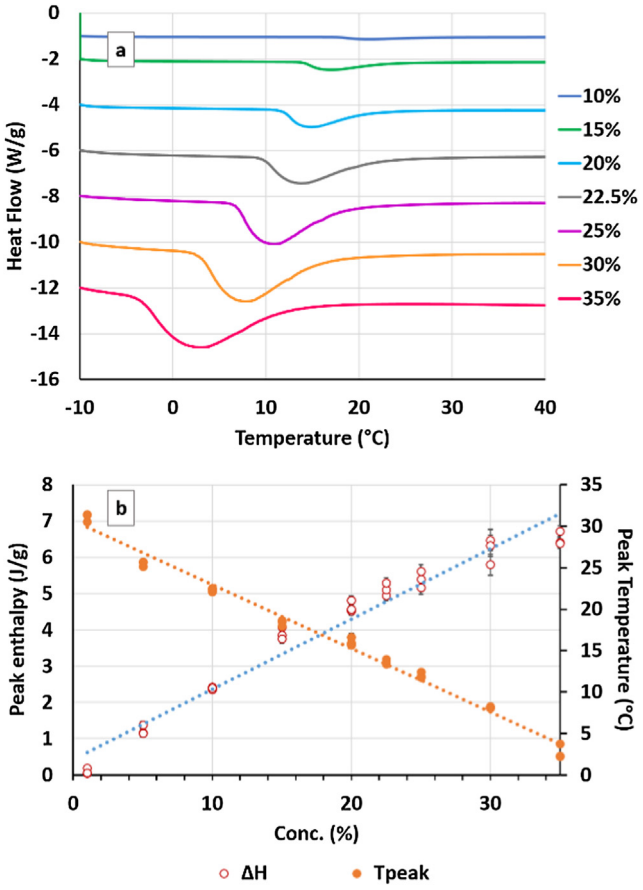

Fig. 1. Thermal analysis results for F127 concentrations ranging from 1 to 30 % performed at a heating rate of 10 °C/min. The range for calculating enthalpy varied according to the transition limits T_{onset} and T_{endset}, which were determined by the inflection method in Trios® software. (a) Thermograms as a function of temperature. Thermograms have been offset by fixed factor of 2 for clarity. (b) Peak temperatures and their respective enthaplies. The curves show results for triplicate runs.

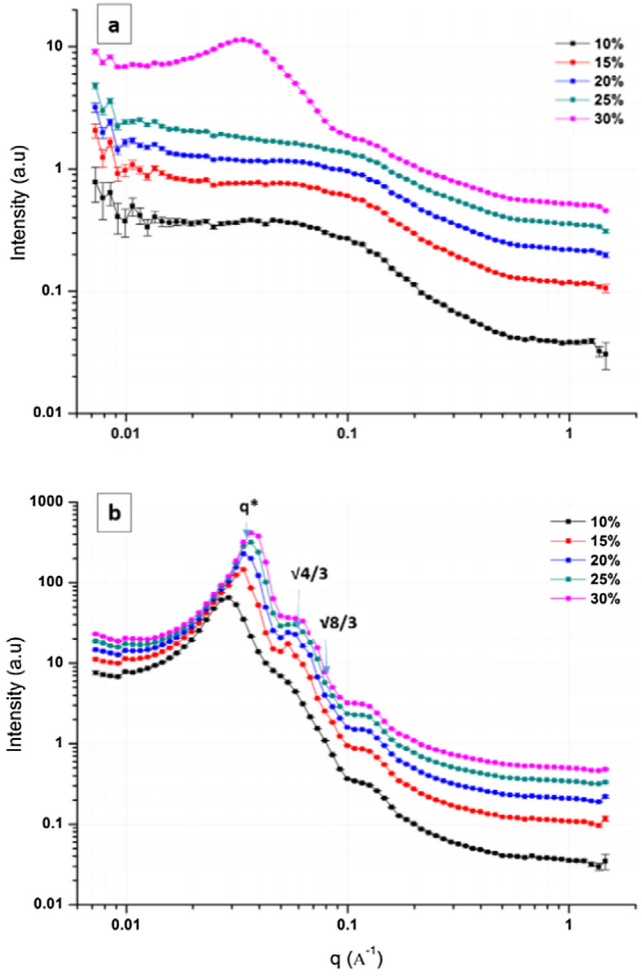

Fig. 2. Static SANS measurements at (a) 5 °C and (b) 37 °C for concentrations of 10 to 30% F127.

detected for 30% at 1, $\sqrt{4}/3$ and $\sqrt{8}/3$ for peak positions of 0.0462, 0.06532 and 0.0766 $Å^{-1}$. Table SI1 shows the measured hard sphere values for the tested concentrations at 37 °C.

3.2. Dynamic measurements

3.2.1. Sol-gel transition

Samples were subjected to four tests with constant shear rate values of 10, 20, 50 and 100 s^{-1} while ramping the temperature from below the transition range (as measured by DSC) to 40 °C. Formulations with low F127 concentrations (1–5%) exhibited reduced viscosity values as the temperature increased with no accompanying shear response (data not shown), and can be considered as Newtonian fluids. As F127 concentration is increased to 10%, a temperature response indicated by a monotonic viscosity reduction up to a temperature of approx. 22 °C, is followed by a viscosity increase up to 31 °C, suggesting a weak structural response that is shear rate independent (results from all four shear rates are overlaid on this plot) [31].

Over the spanned temperature range the rheological properties change dramatically. At low temperatures, F127 15% exhibits similar behaviour to the 10% sample followed by an abrupt tenfold increase in viscosity indicating the gel formation at 28 °C followed by multiple divergence at 29 °C strongly dependent on the shear rate applied. With further temperature increase, the viscosity values remain constant for each applied shear rate value, indicating the formation of a stable temperature independent structures over the temperature range applied. This behaviour is qualitatively similar across the higher concentrations from 15 to 35% as seen in Fig. 4 with viscosity varied as a function of increasing temperature.

Two prominent thermal events can be elucidated from the flow diagrams. Region II in Fig. 3 corresponds to the micellar association taking place in the system, which is due to the increased attraction forces aggregating micelles that grow promptly to form a new structure. For region III, in the same figure, the phase change is confirmed by the significantly different rheological behaviour of the final matrix which exhibit significantly higher viscosity values (three decade increase) when compared to the micellar fluid existent at lower temperatures. Here the formulations exhibit a clear shear dependency demonstrated by the shear thinning behaviour at identical thermal conditions, where $\eta_{10\ s^{-1}} > \eta_{20\ s^{-1}} > \eta_{50\ s^{-1}} > \eta_{100\ s^{-1}}$. Both the transition onset

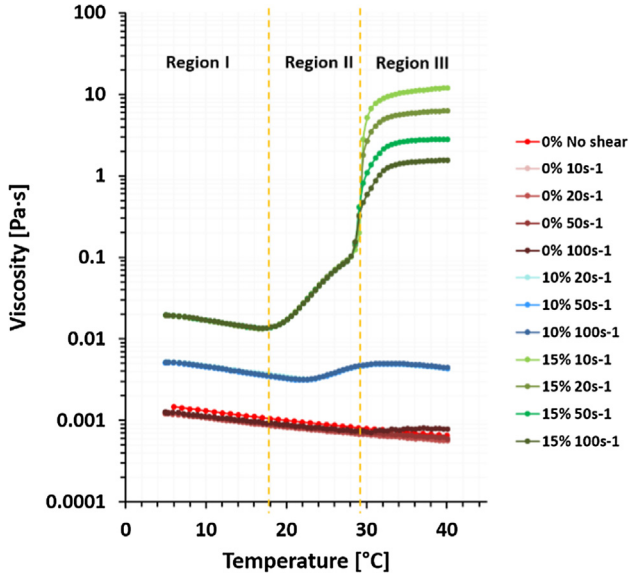

Fig. 3. Temperature ramps at constant shear rates on samples of concentrations 0, 10 and 15% F127. Pure water's no shear viscosity is taken from [31].

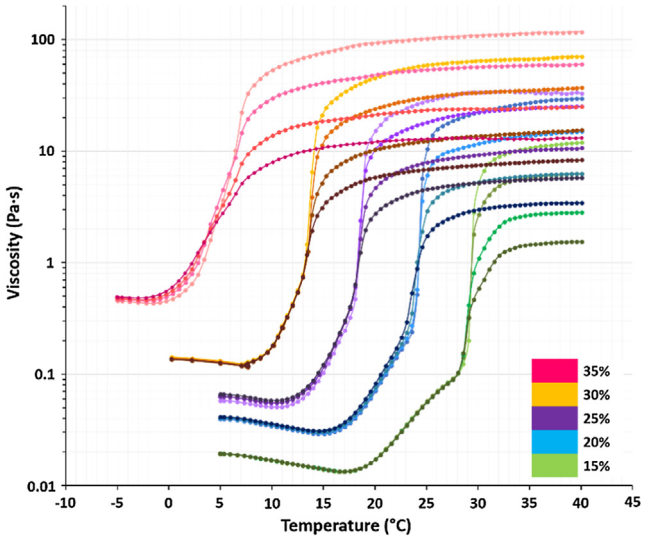

Fig. 4. Temperature ramps at constant shear rates. Each sample concentration was measured at four different shear rates: 10, 20, 50 and 100 s^{-1}. In Region III the viscosity values decrease with shear rate.

temperature and the final viscosity values are proportional to F127 concentration. Data collected during dynamic rheological measurements were found well aligned with the static DSC measurements under the same heating rate as seen for the sample containing 20% F127 in Figure SI 3.

The overall formulations' rheological behaviour across the different temperatures up to gelation can be predicted using a three step series of power law fittings for the different regions of system behaviour. For the first region, 'pre-gel', the formulations are Newtonian and their viscosity is proportional to F127 concentration$C(wt\%)$. η_0 values can be calculated from:

$$\eta_0 = b.C^n + \eta_{water} \tag{2}$$

where b = 7.22×10^{-12} Pa.s , n = 7 and $\eta_{water} = 0.001$ Pa.s

In region II or 'gel transition', from the gelation 'kick off' to the shear dependent divergence point, each formulation's rheology is solely temperature dependent allowing the determination of the gelation transition temperature from:

$$T_{gel} = dC^2 - l \tag{3}$$

where d = 0.02 °C and l = 33.2 °C

This expression can be combined with Eq. (4) to calculate the corresponding viscosity values for any temperature η_T in this region up to the gelation point:

$$\eta_T = \eta_0\left[k + s\left(\frac{T}{T_{gel}}\right)^p\right] \tag{4}$$

where k = 0.15, s = 6.12 and p = 5.6

Performing shear ramps above gelation at 37 °C confirmed the yield stress property of the systems and revealed a non-monotonic stress response that extends over the broad shear rates range investigated (0.001–1500 s^{-1}) as shown in Fig. 5. Gels exhibited a stress drop after a start-up overshoot observed at low shear rates (0.01 s^{-1}). Although the Herschel-Bulkley (HB) model ($\tau = K\dot{\gamma}^n + \tau_0$) provides a good description for the overall material behaviour, it fails to predict the irregular shear stress response across the different regions of the tested range. These irregularities could manifest from inhomogeneous flow in the Couette shear gap which resembles similar shear banding trends reported in other Pluronics [32,33].

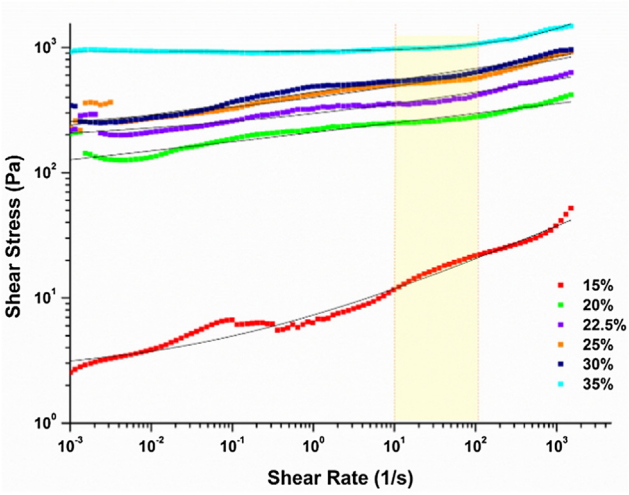

Fig. 5. F127 shear ramps at 37 °C. Black lines represent the Herschel-Bulkley fits for each respective concentration. The highlighted region (10–100 s^{-1}) represent the limits of the modelling.

The resultant flow curves for the shear rates of interest (10–100 s^{-1} highlighted in Fig. 5) show a more uniform behaviour compared to very low/high shear rates. When fitted using the HB model concentrations from 20 to 30% exhibited the same trends with a yield stress correlating to the formulation's concentration, whereby:

$$\tau = \tau_0 + j\dot{\gamma}^{0.1} \quad (5)$$

where j = 110 Pa.s , $\tau_0 = uC^2 - w$ with u = 0.88 Pa.s and w = 264. 56 Pa.s

The fittings for the highest concentration used 35% deviated from the power law registered values, but still exhibited the same trend. Graphs showing the fit quality for each region with their respective R^2 values are displayed in Figure SI 4.

3.2.2. Frequency sweeps

Oscillatory frequency sweeps were conducted at 37 °C from 0.001 to 100 rad/*sec*, as plotted in Fig. 6. The gels showed an overall dominance of G' weakly dependent on the frequency applied. The loss moduli for the samples decrease with increasing frequency. This G' > G" motif across the whole frequency range confirms the gel stability and implies that all samples except 15% have undergone their micelle to hard sphere transition, similar to that observed by Li et al [34]. From the higher concentration group shown in Fig. 6 only the 15% sample exhibited a cross-over point at ω = 0.0063 rad/*sec*; the rest of the concentrations showing no indication of relaxation within the experimental time (ca. 5 h). Extended measurements were conducted to reduce the instrumental noise at low frequencies (run time up to 12 h) with no significant moduli differences. The elastic response for concentrations higher than 15% was found to follow the relationship $G' \sim \omega^{\beta}$, with exponent β of 0.05 and G"/G'~ O (0.1), two features common in soft glassy materials [35].

3.2.3. Temperature sweeps

The dynamic moduli variation with temperature was studied under oscillatory mode within the linear viscoelastic region. As seen in Fig. 7-a, at low temperatures, formulations containing 22.5 to 35% F127 exhibit low moduli values with G" > G'. At a critical temperature both moduli values increase and G' and G" cross over. This is followed by an extended plateau before the moduli values decrease upon reaching another critical temperature. The two critical temperatures marking the crossover points are defined as the gel boundaries, where the lower gelation boundary (LT_{gel}) is assigned to the first crossover point indicating the gel structure formation and upper gelation boundary (UT_{gel}) to the second crossover for its destruction. In the case of 15% F127 the formulation was observed to regain its solution state, reaching almost the same start-up values of G' and G".

The gelation 'window' was found to be strongly dependent on F127 content, with higher concentrations exhibiting a broader range of ($UT_{gel} - LT_{gel}$). The acquired limits show good agreement to published values as shown in Fig. 7-b [36].

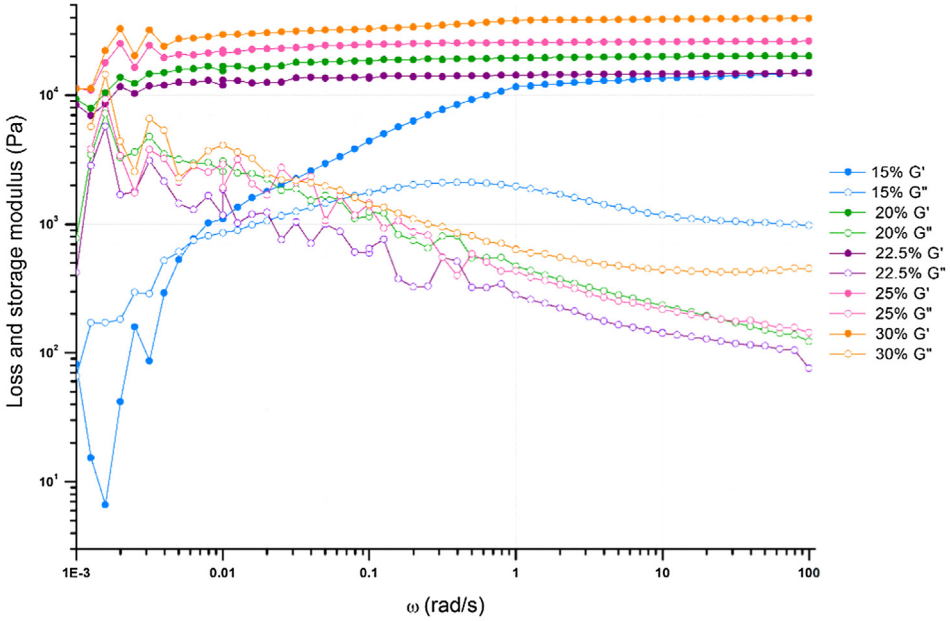

Fig. 6. Frequency sweeps at 37 °C from 0.001 to 100 rad/*sec* at strain amplitude of 0.2%.

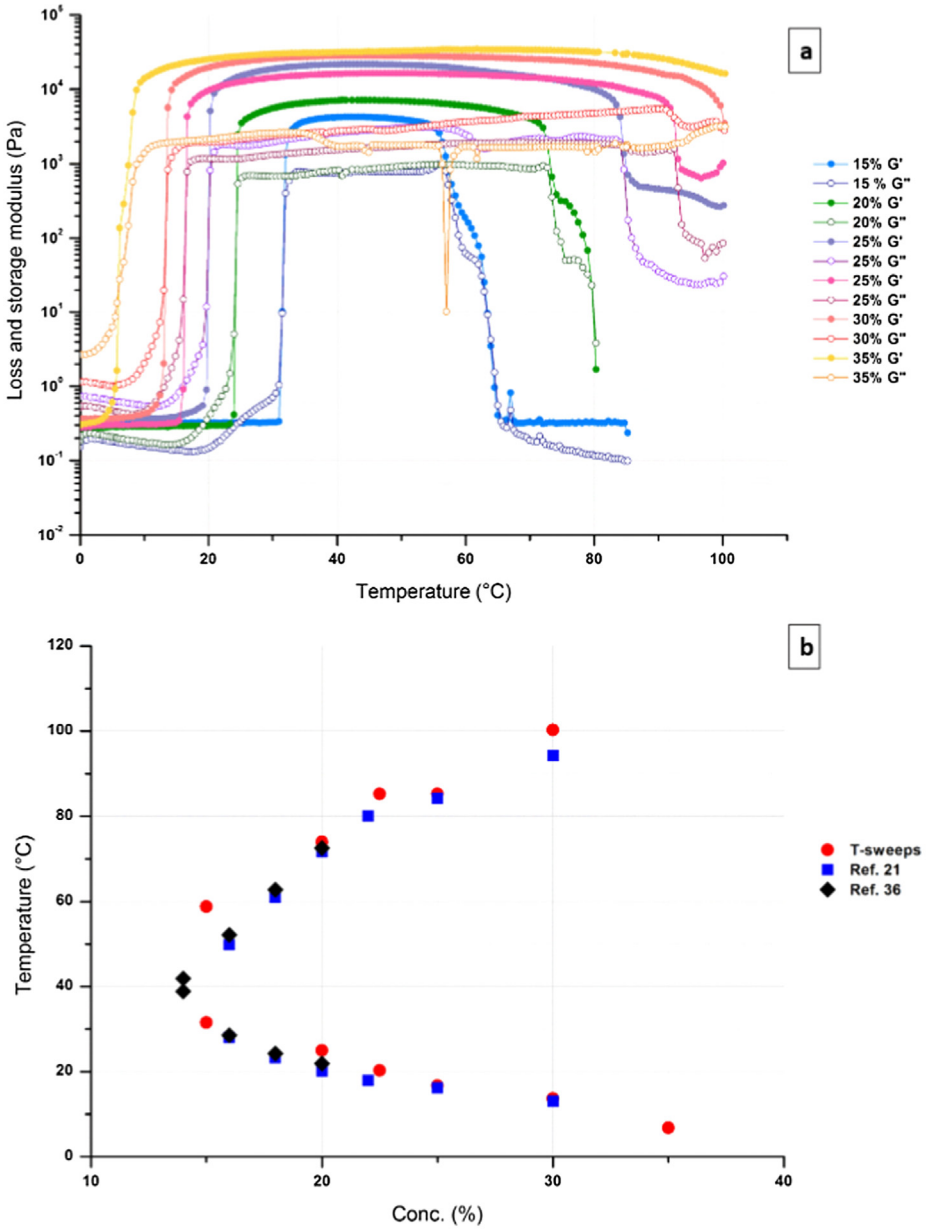

Fig. 7. F127 temperature sweep results showing (a) dynamic moduli variation with temperature and (b) gelation limits determined from Fig. 7-a compared to recent studies' values.

3.3. Rheo-SANS

For the Rheo-SANS measurements, samples at three different concentrations were sheared at temperatures below their gelation, during gelation and at 37 °C. Below gelation, as expected, the polymeric solutions do not exhibit any structural ordering and the results were identical to SANS results from static samples. At their respective values of T_{gel}, samples showed similar 1D scattering profiles to those recorded in static measurements in Fig. 2 with slight shifts to lower q-values - see Figures SI 5–6. The flow behaviour of deuterated F127 systems did not show significant differences to undeuterated systems used throughout the study, except for the slightly higher viscosities recorded for the former as seen in Figure SI 12, these being commensurate with the higher viscosity of D_2O compared to H_2O.

The effect of shear is clear in the anisotropic 2D scattering profiles. The recorded structures under both shear rates (10 and 100 s^{-1}) were found to correspond to positions in both FCC and HCP crystals. In 20% F127 these correspond to recorded q values of FCC and HCP structures: $\sqrt{3}$ (FCC), $\sqrt{4}$ (FCC/HCP), $\sqrt{20/3}$ (FCC), $\sqrt{12}$ (FCC). Similar fittings were acquired for higher concentrations of 25 and 30% F127.

For gelation transitions, at low shear rate (10 s^{-1}), the gels demonstrate a six fold symmetry with slightly higher intensity in the meridional Bragg peaks in comparison to the remaining four side peaks, as observed in Fig. 8-a.

When the shear rate was increased to 100 s^{-1} at the same temperature, the previously seen anisotropy in the 25% sample was replaced by another structure with a reduced intensity in the meridional peaks in comparison to the remaining four peaks, as seen in Fig. 8-b.

After gelation, at 37 °C, less prominent differences were displayed with a ubiquitous six fold symmetry - higher meridional peak intensity, suggesting that this morphological structure is

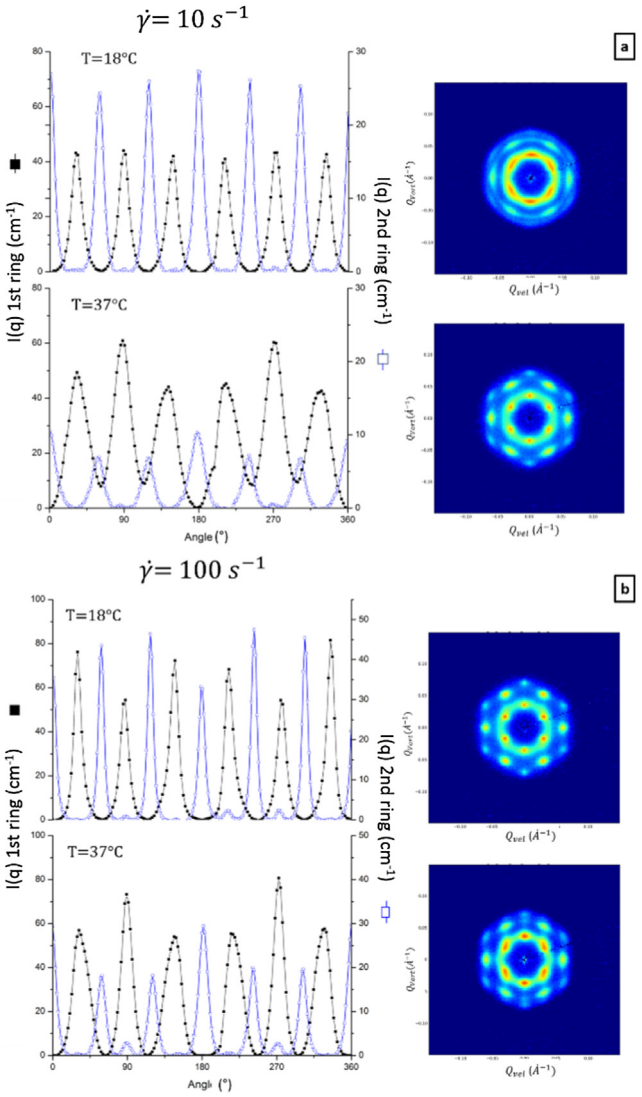

Fig. 8. Rheo-SANS azimuthal scattering profiles for 25% F127 at the gel transition and 37 °C under (a) 10 s^{-1} and (b) 100 s^{-1}.

the final and most stable over the applied temperature range, even after the application of high shear rates, see Fig. 8.

Annular profiles of F127 30% resembled those obtained for 20 and 25% F127 at the transition temperature and 37 °C under 10 s^{-1}. However, when 100 s^{-1} was applied the meridional peaks demonstrated higher intensities at both temperatures as seen in Figure SI 9 and 10.

According to the most widely used model for sheared close packed colloidal structures, from Loose and Ackerson [37], the FCC crystals undergo a transition to form two-dimensional hexagonal close packed (2D-HCP) layers to minimise resistance to flow. The respective final structures depend on the extent of the shear rate applied, with low shear rates resulting in a zigzag planar trajectory while higher $\dot{\gamma}$ values produce a sliding motion. In 2D scattering azimuthal profiles this corresponds to reduced intensity of the top and bottom peaks for zigzag motion and their complete disappearance for the sliding mechanism [30]. Similar azimuthal profiles to those in Fig. 8-b were obtained by Pozzo and Walker [30] for gels of F127 25% at 25 °C (above gelation temperature but before the gel plateau) under 100 s^{-1}.

The appearance of the four fold symmetry in the second ring led them to suggest that the system might be close to the sliding layer prediction and they theorised that the peaks were a result of the coexistence of multiple crystal orientations within the shear gap: FCC and HCP, while the sliding layers model was based on a single orientation of the entire sample. We make similar conclusions supported by the results from a much broader sample range tested and presented here, where most of the samples displayed different 1st and 2nd ring structures, indicating the possibility of the formation of multiple structural orientations within the shear gap by different mechanisms.

Jiang *et al.* [38] studied 20% F127 gel at different shear rates from 0.01 to 600 s^{-1}, and reported the formation of 2D-HCP stacks in the shear plane with 2D profiles similar to the recorded Rheo-SANS data presented here, though no azimuthal analysis was published. Lopez-Barron *et al.* [39] obtained four high intensity spots with shear rates from 1 to 500 s^{-1} for a solution of F127 24% in deuterated ionic solvent ethylammonium nitrate (dEAN) at 40 °C, before the sample reached full isotropy due to shear melting.

The reported differences between the current study and the aforementioned works highlight the structural variation arising from solvent change. The diffraction patterns acquired for sheared gels after cooling indicated a complete reversibility to the solution state with identical signals to those recorded for static measurements at 5 °C, as shown in Figure SI 11.

The average full width of half maximum (FWHM) values of each azimuthal Rheo-SANS scan at the meridional positions are used to quantify the orientation at the two temperatures of interest in Fig. 9. Regardless of temperature, higher shear was more effective in producing a higher degree of orientation (lowest FWHM values). The plotted results highlight that for T_{gel}, the orientation increases as a function of concentration under 10 s^{-1} while at 100 s^{-1}, the opposite trend is observed with lower concentrations experiencing higher degrees of orientation. Since only the meridional position averaged FWHM values were used for this analysis, the results cannot provide a fully accurate representation of the orientation owing to the gels containing 20 and 25% F127 demonstrating different symmetries to those for the 30% F127 sample at T_{gel} and under 100 s^{-1}.

The fourfold symmetry seen at T_{gel} and higher shear rates matches with the Loose and Ackerson model prediction, indicating a zig-zag movement. The reoccurring patterns observed at the lower shear rate during and after gelation are not however predicted by the same model, where the top and bottom peaks in

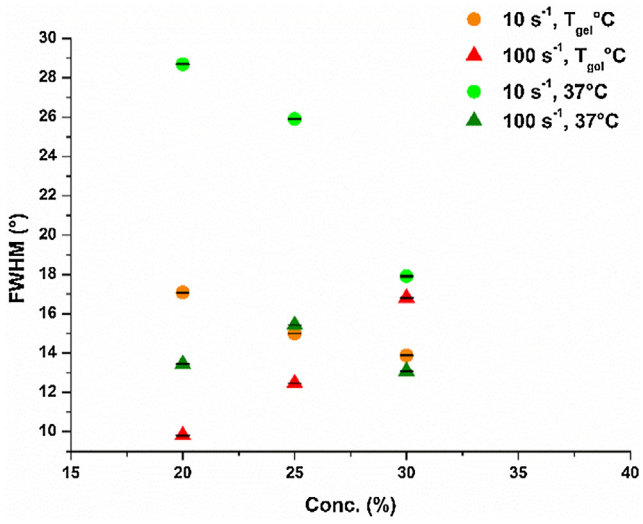

Fig. 9. Variation in calculated FWHM values with F127 concentration at 37 °C at gelation and body temperatures for two shear rates.

the first hexagon show higher intensity than the four sided peaks rather than their predicted disappearance.

Experiments performed on another shear banding gelling system of a lower molecular weight, Pluronic F68 at 46% that forms BCC structures, have demonstrated the existence of three coexisting orientations as a result of a layer slip mechanism imposed by an intermediate shear rate of 50 s^{-1} [40], showing similar qualitative results to the present study.

Comparison of unit cell size (a_{FCC}) between sheared and static gels shown in Fig. 10 reveals higher copolymer concentrations result in the formation of more densely packed hard spheres. At low shear (10 s^{-1}) the a_{fcc} values are very close to those for static conditions while at 100 s^{-1} shear clearly causes a decrease in unit cell size.

The results of coupled scattering and rheological measurements under different shear rates, temperatures and using multiple concentrations allows for further analysis. The thermal, structural and rheological terms can be combined to calculate the Peclet number (Pe) [41] where:

$$Pe \equiv 6\pi\eta_0\dot{\gamma}a^3/k_BT \quad (7)$$

Here, the rheological conditions are represented by η_0, the zero shear viscosity (initial) and $\dot{\gamma}$, the shear rate applied. a is the particle radius from scattering (using the hard sphere radius values). The thermal conditions are represented by k_BT, the Boltzmann constant and the applied temperature, respectively. The calculated Peclet number values are plotted as a function of shear stress and are presented in Fig. 11. The datasets can be fitted using the universal power law:

$$\tau = kPe^n \quad (8)$$

where k = 6010.7 J/m^3 = Pa and n = 0.89

With elevation of temperature, this plot highlights the gelled system's sensitivity to shear rate. Higher concentrations display higher viscosities and have higher packing density but, rheologically, they respond to the shear in a similar fashion to the lower concentrations as depicted by the trend line. The gradient of the curve represents the relationship between temperature and the hard sphere radius - which is a function of shear and concentration (T/a^3). This indicates the logarithmic scalability of the thermo-rheological response of the gels. Prior knowledge of shear conditions would thus be sufficient to determine the hard sphere particle size making up the crystal lattice and vice versa if the sphericity is maintained.

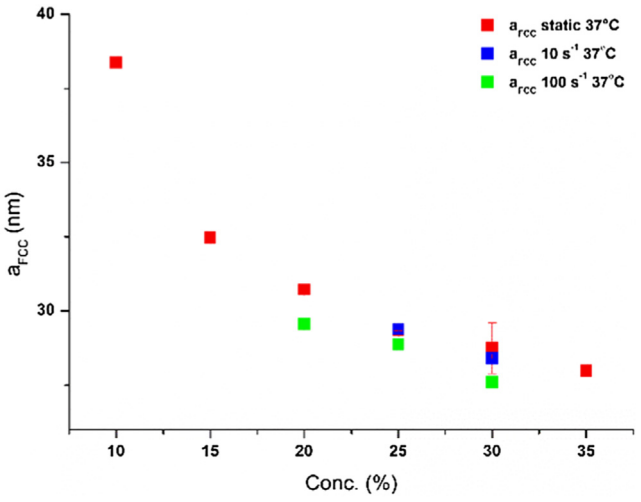

Fig. 10. Variation in F127 unit cell values calculated from SANS experiments: static and under imposed shear at 37 °C, with concentration. The uncertainty bars for the unit cell parameter are hidden behind the data symbols. All values are provided in Table S1.

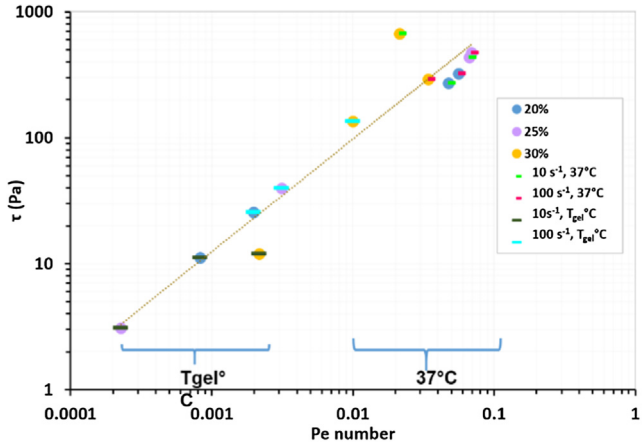

Fig. 11. Calculated Peclet numbers for F127 formulations from the Rheo-SANS data with their respective shear stress values.

3.4. Rheo-SAXS

3.4.1. Steady-shear SAXS

Fig. 12 shows the rheological measurements at 10 s^{-1} on 25% F127 using the Couette cylinder geometry overlaid with the matching 2D SAXS patterns recorded during the application of rotational shear with a heating rate of 2 °C/min.

The system exhibits a reduced viscosity with a weak halo at 10 °C indicating the micellar state which, according to DSC thermograms, commences at around 8 °C. Upon reaching the transitional stage at 13 °C, two faint rings appear, increasing in intensity as the rheological divergence point is approached at 18 °C. This coincides with strong structures as depicted by two Bragg rings, with high intensity in the equatorial and meridional peaks, in the first and second rings, respectively. Above 27 °C, the viscosity is weakly temperature dependent, but the structure continues to become more ordered as implied by the continuing intensity increase in both rings. However this ceases at 40 °C where the recorded scattering is predominantly from the first ring peaks showing almost symmetric intensities across the hexagonal spots. Further increase in temperature to 49 °C – still within the gelation window according to Fig. 7–a, resulted in a structural change, where the first ring's four sided peaks became stronger, consistent with the zig-zag motion predictions at low shear rates [30,42]. The results of these experiments demonstrate the possibility of structural transition from the high intensity at top and bottom positions to the four sided anisotropy; a transition observed in the Rheo-SANS high shear runs through temperature increase (Fig. 8).

3.4.2. Mixed-shear SAXS (syringe pump)

The samples were loaded into a syringe at 5 °C to be injected under different shear rates (from 1 to 90 s^{-1}) into an x-ray transparent channel at room temperature (23 °C) and measurements taken every 60 s following injection.

Fig. 13 shows the structural development of 25% F127 injected at 10 s^{-1}. The sample 1D profile shows three peaks at positions of 0.0536, 0.064 and 0.0726 $Å^{-1}$ that merge to form a dominant peak at 0.07 $Å^{-1}$ by the end of the test. This slight shift indicates a loosening of the structure and reversion to a state of reduced order. In

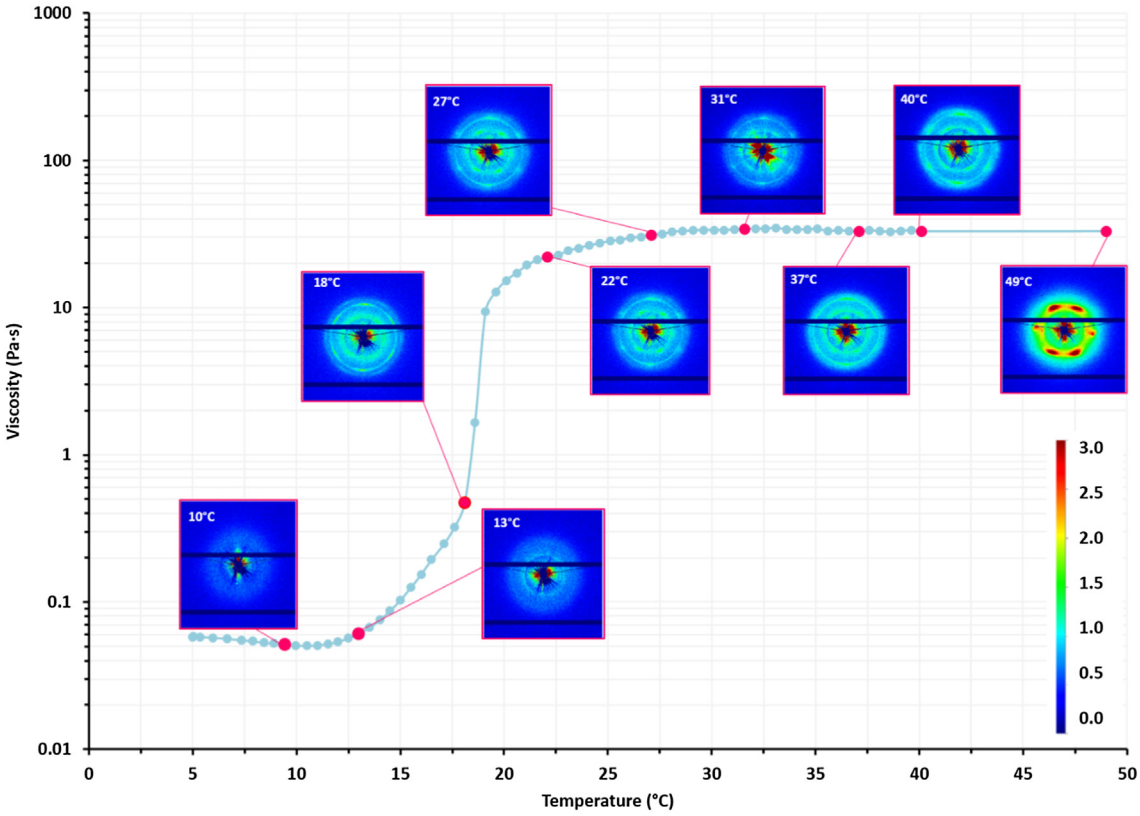

Fig. 12. SAXS data collected using Linkam shear cell during temperature ramps for 25% F127 under constant shear of 10 s^{-1}. The horizontal black bands in the 2D SAXS scattering images are due to inter-module gaps of the detector.

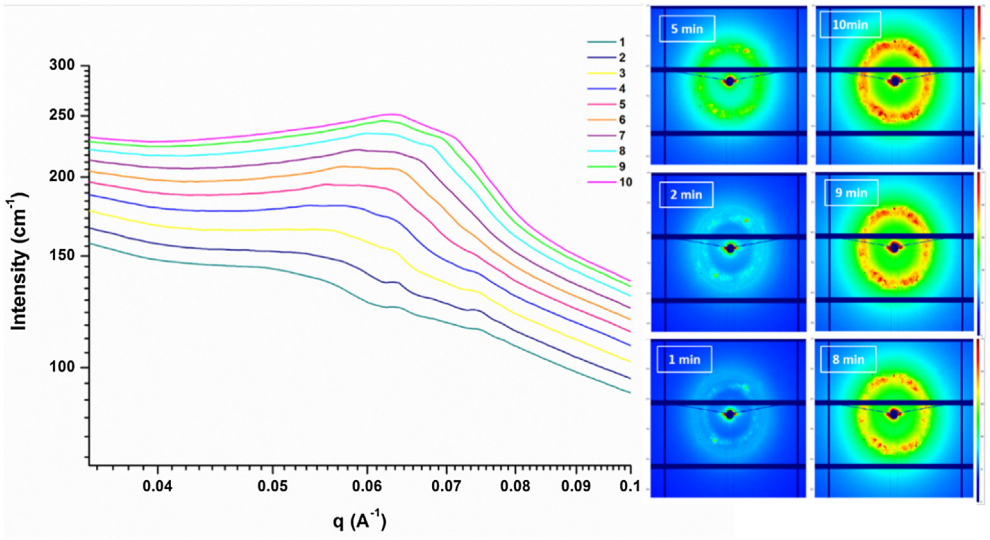

Fig. 13. SAXS profiles for 25% F127 tested using syringe pump injection at 10 s^{-1} where the legend represents the time in minutes. The horizontal black bands in the 2D SAXS scattering images are due to inter-module gaps of the detector.

the corresponding 2D scattering patterns, two strong spikes appear in the position where a Bragg peak would be expected, accompanied by further growth in the intensity at positions of the four side peaks that spread omni-directionally in the first ring.

At the highest shear rate applied, 90 s^{-1} with the highest concentration tested (30% F127), the 1D plots exhibit highly ordered structures from the start of the measurements with peaks at 0.041, 0.046, 0.071 and 0.08 $Å^{-1}$. These peaks fuse into one main peak with a q value of 0.06 $Å^{-1}$ and an intensity almost twice higher than the q* as shown in Fig. 14.

The shear and combined extensional flow effects observed in the results section lead to the following conclusions:

(1) The resultant structure is highly ordered after injection, demonstrated by the sharpness of 1D peaks and strong defined scattering in 2D, where the scattering intensity is a function of concentration.
(2) The injection process results in the formation of spikes not present in the steady shear experiments. These spikes correspond to locally more ordered domains which seed

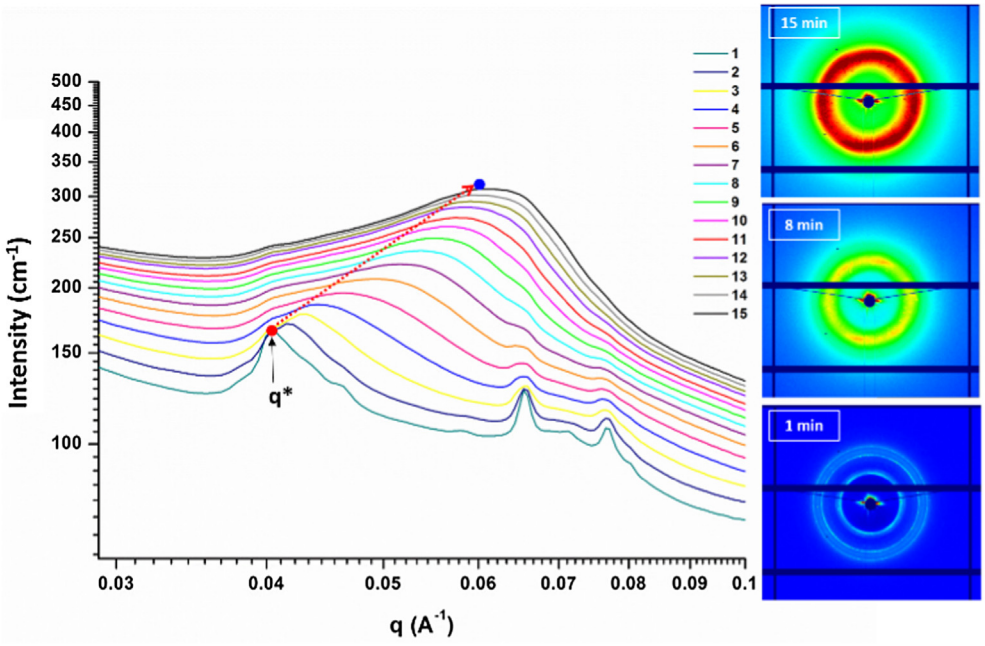

Fig. 14. SAXS profiles for 30% F127 tested using syringe pump injection at 90 s^{-1} where the legend represents the time in minutes. The horizontal black bands in the 2D SAXS scattering images are due to inter-module gaps of the detector.

heterogeneous nucleation. Their distribution appears to be spatially linked to the disordered manner of their initiation giving the scattering pattern a hazy speckled look. There have been no accounts in Pluronics literature documenting this phenomenon after injection, although some groups have reported the appearance of temporary spikes under static conditions which disappeared after heating above 50 °C [27,29]. The origin of the initial spike formation is likely to be connected to the unhomogenised flow arising in the channel accompanied by the continuous temperature change throughout the injection process, however the propagation of the spikes would be expected to be a product of temperature after shear cessation.

Fig. 15 shows the time-resolved peak positions and their respective intensity progression recorded after different shear rates (1, 10 and 90 s^{-1}) for the sample containing 30% F127. From the peak positions in Fig. 15-a, it can be seen that q* shifts to the higher q-values as the small peaks merge together indicating a reduction in domain sizes, accompanied by a steady increase in scattering intensity in Fig. 15-b signifying the continuous formation of ordered structures. The fitted peak values are similar for 10 and 90 s^{-1} while the recorded scattering intensities are initially inversely proportional to the shear rate applied. Over the time of the whole test however, the final values become independent of this shear rate.

Based on the results indicating an ordered close packed structure and with final elliptical structures formed after shear cessation, it is suggested that the micelles may lose their initial isotropy as a result of flow application, leading to induced orientation in the injection direction. As shear is ceased two events are expected: (a) the gel structure will relax in the nearest registry site to the shear aligned position, (b) since the temperature is lower than required to maintain the stable gel structure, the gel will revert back to a weaker gel state ending in a mixed state of coexisting order-disorder. In this case hexagonal and cubic structures are formed within the same matrix with extra spikes indicating a defected lattice. These conclusions are supported by the peak merging and the close proximity of registered peak positions observed, even after the application of different magnitudes of shear rate.

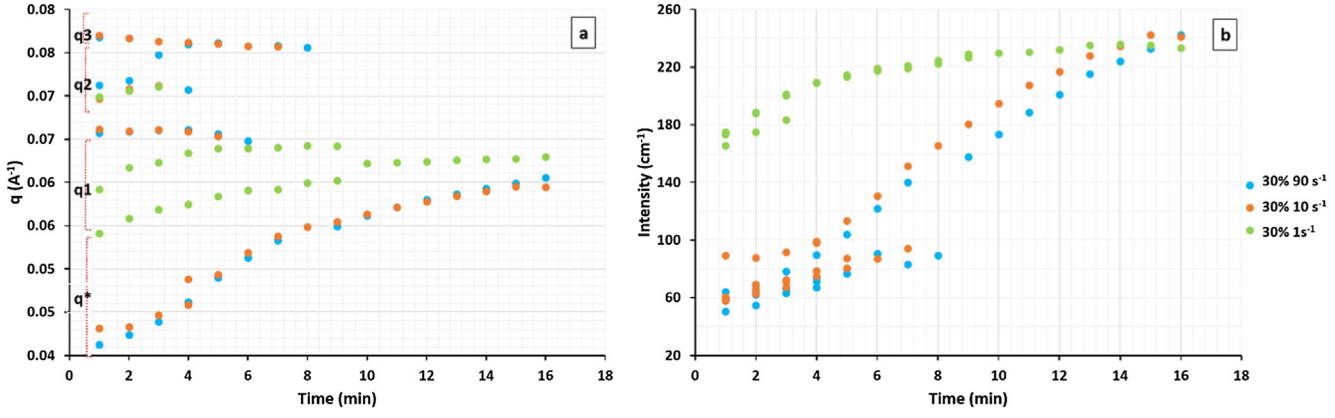

Fig. 15. Progression of (a) scattering vector and (b) intensity values acquired for injected 30% F127 at three different shear rates.

4. Conclusions

This paper presents a comprehensive study of the thermal, rheological and structural properties of F127 systems with the aim to provide experimental guidelines for future development of DDSs containing Pluronics or their smart colloidal analogues. The properties of a wide range of concentrations (F127 1–35%) were examined using novel experiments combining rheological investigation with small angle x-ray and neutron scattering.

The investigated systems at concentrations above 15% were proven to undergo a reversible thermal transition from easy to handle micellar liquids to shear thinning physical gels making them ideal for injectable drug delivery applications.

We presented a set of empirical rules that predict the gelling system's rheological behaviour of any F127 concentration above 20% during the three stages it undergoes as a function of temperature and shear rate.

The study elucidated that macroscopic shear response after gelation is a direct result of the structural alignment of the gel hard sphere layers in the shear direction, which, based on the rheo-scattering experimental results, will depend on the applied flow type and its extent as quantified by the results for steady shear and combined flow. The systems structural reversibility was confirmed by all three method in this study, whether shear was applied or not.

The scattering patterns obtained for the oriented systems highlighted the capability of flow to reduce crystal unit cell size and suggests the existence of more than one orientation as a result of flow, in agreement literature on the mixed phase orientation phenomenon in similar sheared colloidal crystals [30,40].

These quantified non-equilibrium effects are critical to model the system's syringeability/ injectability during clinical use as well as the loaded drug deposition within the crystalline matrix. This allows for the utilisation of the injection speed to manipulate the drug release profile inside the body.

Further in vitro/vivo investigations are under way to quantify the implications of flow driven structural changes on the overall behaviour on a model drug delivery system.

CRediT authorship contribution statement

Bana Shriky: Conceptualization, Methodology, Investigation, Formal analysis, Writing - original draft. **Adrian Kelly:** Writing - review & editing. **Mohammad Isreb:** Writing - review & editing. **Maksims Babenko:** Investigation. **Najet Mahmoudi:** Data curation, Resources, Writing - review & editing. **Sarah Rogers:** Data curation, Resources. **Olga Shebanova:** Data curation, Resources, Writing - review & editing. **Tim Snow:** Data curation, Resources. **Tim Gough:** Conceptualization, Methodology, Supervision, Writing - review & editing.

Declaration of Competing Interest

The authors declare that they have no known competing financial interests or personal relationships that could have appeared to influence the work reported in this paper.

Acknowledgments

SAXS and SANS beamtimes at STFC- RAL (Didcot, UK) were provided under the experimental proposals 18402 (Diamond), 1790815 and 1800037 (ISIS). The authors are grateful for the assistance of all beamline staff. This work benefited from the use of the SasView (developed under NSF award DMR-0520547) and Dawn softwares.

Appendix A. Supplementary material

Supplementary data to this article can be found online at https://doi.org/10.1016/j.jcis.2019.12.096.

References

[1] N. Bhattarai, J. Gunn, M. Zhang, Chitosan-based hydrogels for controlled, localized drug delivery, Adv. Drug Deliv. Rev. 62 (2010) 83–99, https://doi.org/10.1016/j.addr.2009.07.019.
[2] M. Ebara, Y. Kotsuchibashi, K. Uto, T. Aoyagi, Y.-J. Kim, R. Narain, N. Idota, J.M. Hoffman, Smart Hydrogels, in: Smart Biomater, Springer, Japan, Tokyo, 2014, pp. 9–65. https://doi.org/10.1007/978-4-431-54400-5_2.
[3] J.M. Barichello, M. Morishita, K. Takayama, T. Nagai, Absorption of insulin from Pluronic F-127 gels following subcutaneous administration in rats, Int. J. Pharm. 184 (1999) 189–198, https://doi.org/10.1016/S0378-5173(99)00119-2.
[4] S.S. Dewan, B.C.C. research, Global Markets and Technologies for Advanced Drug Delivery Systems – Focus on Routes of Administration, (2014). https://www.bccresearch.com/market-research/pharmaceuticals/advanced-drug-delivery-administration-phm165a.html.
[5] A. Hatefi, B. Amsden, Biodegradable injectable in situ forming drug delivery systems, J. Control. Release. 80 (2002) 9–28, https://doi.org/10.1016/S0168-3659(02)00008-1.
[6] C. Alvarez-Lorenzo, A. Concheiro, Smart drug delivery systems: from fundamentals to the clinic, Chem. Commun. 50 (2014) 7743–7765, https://doi.org/10.1039/C4CC01429D.
[7] D. Seliktar, Designing cell-compatible hydrogels for biomedical applications, Science 336 (6085) (2012) 1124–1128, https://doi.org/10.1126/science:1214804.
[8] K.H. Bae, L.-S. Wang, M. Kurisawa, Injectable biodegradable hydrogels: progress and challenges, J. Mater. Chem. B. 1 (2013) 5371–5388, https://doi.org/10.1039/C3TB20940G.
[9] B.A. Aguado, W. Mulyasasmita, J. Su, K.J. Lampe, S.C. Heilshorn, Improving viability of stem cells during syringe needle flow through the design of hydrogel cell carriers, Tissue Eng. Part A 18 (2012) 806–815, https://doi.org/10.1089/ten.tea.2011.0391.
[10] M.H. Amer, F.R.A.J. Rose, K.M. Shakesheff, M. Modo, L.J. White, Translational considerations in injectable cell-based therapeutics for neurological applications: concepts, progress and challenges, Npj Regen. Med. 2 (2017) 23, https://doi.org/10.1038/s41536-017-0028-x.
[11] A.M. Pragatheeswaran, S.B. Chen, Effect of chain length of PEO on the gelation and micellization of the pluronic F127 copolymer aqueous system, Langmuir 29 (2013) 9694–9701, https://doi.org/10.1021/la401639g.
[12] M. Valero, F. Castiglione, A. Mele, M.A. da Silva, I. Grillo, G. González-Gaitano, C. A. Dreiss, Competitive and synergistic interactions between polymer micelles, drugs, and cyclodextrins: the importance of drug solubilization locus, Langmuir 32 (2016) 13174–13186, https://doi.org/10.1021/acs.langmuir.6b03367.
[13] C.M. de Lima, S.M.C. Siqueira, A.F.V. de Amorim, K.B.S. Costa, D.H.A. de Brito, M. E.N.P. Ribeiro, N.M.P.S. Ricardo, C. Chaibunditc, S.G. Yeates, N.M.P.S. Ricardo, Effects of polypropylene glycol 400 (PPG400) on the micellization and gelation of pluronic F127, Macromolecules (2015), https://doi.org/10.1021/acs.macromol.5b01655.
[14] P. Alexandridis, T. Alan Hatton, Poly(ethylene oxide)-poly(propylene oxide)-poly(ethylene oxide) block copolymer surfactants in aqueous solutions and at interfaces: thermodynamics, structure, dynamics, and modelling, Coll. Surf. A Physicochem. Eng. Asp. 96 (1–46) (1995), https://doi.org/10.1016/0927-7757(94)03028-X.
[15] A.M. Bodratti, P. Alexandridis, Formulation of poloxamers for drug delivery, J. Funct. Biomater. 9 (2018) 11, https://doi.org/10.3390/jfb9010011.
[16] G. Wanka, H. Hoffmann, W. Ulbricht, The aggregation behavior of poly-(oxyethylene)-poly-(oxypropylene)-poly-(oxyethylene)-block-copolymers in aqueous solution, Coll. Polym. Sci. 268 (1990) 101–117, https://doi.org/10.1007/BF01513189.
[17] K. Mortensen, Y. Talmon, Cryo-TEM and SANS microstructural study of pluronic polymer solutions, Macromolecules 28 (1995) 8829–8834, https://doi.org/10.1021/ma00130a016.
[18] I.W. Hamley, Block copolymers in solution: fundamentals and applications, Wiley, 2005. https://books.google.co.uk/books?id=OcOd6o_0YSUC.
[19] I.W. Hamley, Amphiphilic diblock copolymer gels: the relationship between structure and rheology, Philos. Trans. Math. Phys. Eng. Sci. 359 (2001) 1017–1044. http://www.jstor.org/stable/3066551.
[20] K. Mortensen, W. Batsberg, S. Hvidt, Effects of PEO−PPO diblock impurities on the cubic structure of aqueous PEO−PPO−PEO pluronics micelles: fcc and bcc ordered structures in F127, Macromolecules 41 (2008) 1720–1727, https://doi.org/10.1021/ma702269c.
[21] C.C. Hopkins, J.R. de Bruyn, Gelation and long-time relaxation of aqueous solutions of Pluronic F127, J. Rheol. (N. Y. N. Y). 63 (2019) 191–201, https://doi.org/10.1122/1.5054598.
[22] I.R. Schmolka, Artificial skin I. Preparation and properties of pluronic F-127 gels for treatment of burns, J. Biomed. Mater. Res. 6 571–582 (1972). https://doi.org/doi:10.1002/jbm.820060609.
[23] Anton-Paar, RheoOptics - Rheo-SANS/SAXS Small-Angle Neutron or X-ray Scattering, 2019. https://www.anton-paar.com/uk-en/products/details/rheooptics-rheo-sanssaxs-small-angle-neutron-or-x-ray-scattering/.

[24] STFC-ISIS, MCR501 Rheo-SANS Couette Cell, (2018). https://www.isis.stfc.ac.uk/Pages/sans-rheometer-cell-dimensions9812.pdf.
[25] M. Zhang, M. Djabourov, C. Bourgaux, K. Bouchemal, Nanostructured fluids from pluronic® mixtures, Int. J. Pharm. 454 (2013) 599–610, https://doi.org/10.1016/j.ijpharm.2013.01.043.
[26] L.C. Pham Trong, M. Djabourov, A. Ponton, Mechanisms of micellization and rheology of PEO–PPO–PEO triblock copolymers with various architectures, J. Coll. Interf. Sci. 328 (278–287) (2008), https://doi.org/10.1016/j.jcis.2008.09.029.
[27] Robert K. Prud'homme, Guangwei Wu, Dieter K. Schneider, Structure and rheology studies of poly(oxyethylene−oxypropylene−oxyethylene) aqueous solution, Langmuir 12 (20) (1996) 4651–4659, https://doi.org/10.1021/la951506b.
[28] J. Jiang, C. Li, J. Lombardi, R.H. Colby, B. Rigas, M.H. Rafailovich, J.C. Sokolov, The effect of physiologically relevant additives on the rheological properties of concentrated Pluronic copolymer gels, Polymer (Guildf 49 (2008) 3561–3567, https://doi.org/10.1016/j.polymer.2008.05.038.
[29] N.A.K. Meznarich, B.J. Love, Effect of ternary solutes on the evolution of structure and gel formation in amphiphilic copolymer solutions, The University of Michigan, 2012.
[30] D.C. Pozzo, L.M. Walker, Shear orientation of nanoparticle arrays templated in a thermoreversible block copolymer micellar crystal, Macromolecules 40 (2007) 5801–5811, https://doi.org/10.1021/ma0700173.
[31] Anton-Paar, Viscosity of Water, (2019). https://wiki.anton-paar.com/en/water/.
[32] T.G. Mezger, The rheology handbook : for users of rotational and oscillatory rheometers, 3rd ed., Vincentz Network GmbH & Co KG, Hannover, 2011.
[33] E. Eiser, F. Molino, G. Porte, X. Pithon, Flow in micellar cubic crystals, Rheol. Acta. 39 (2000) 201–208, https://doi.org/10.1007/s003970000083.
[34] X. Li, E. Park, K. Hyun, L. Oktavia, M. Kwak, Rheological analysis of core-stabilized Pluronic F127 by semi-interpenetrating network (sIPN) in aqueous solution, J. Rheol. (N. Y. N. Y) 62 (2017) 107–120, https://doi.org/10.1122/1.5009202.
[35] D.T.N. Chen, Q. Wen, P.A. Janmey, J.C. Crocker, A.G. Yodh, Rheology of soft materials, Annu. Rev. Condens. Matter Phys. (2010).
[36] X. Li, K. Hyun, Rheological study of the effect of polyethylene oxide (PEO) homopolymer on the gelation of PEO-PPO-PEO triblock copolymer in aqueous solution, Korea-Australia Rheol. J. 30 (2018) 109–125, https://doi.org/10.1007/s13367-018-0012-z.
[37] W. Loose, B.J. Ackerson, Model calculations for the analysis of scattering data from layered structures, J. Chem. Phys. 101 (1994) 7211–7220, https://doi.org/10.1063/1.468278.
[38] J. Jiang, C. Burger, C. Li, J. Li, M.Y. Lin, R.H. Colby, M.H. Rafailovich, J.C. Sokolov, Shear-induced layered structure of polymeric micelles by SANS, Macromolecules 40 (2007) 4016–4022, https://doi.org/10.1021/ma062654j.
[39] C.R. López-Barrón, N.J. Wagner, L. Porcar, Layering melting, and recrystallization of a close-packed micellar crystal under steady and large-amplitude oscillatory shear flows, J. Rheol. (N. Y. N. Y). 59 (2015) 793–820, https://doi.org/10.1122/1.4917542.
[40] E. Eiser, F. Molino, G. Porte, O. Diat, Nonhomogeneous textures and banded flow in a soft cubic phase under shear, Phys. Rev. E. 61 (2000) 6759–6764, https://doi.org/10.1103/PhysRevE.61.6759.
[41] R.G. Larson, The structure and rheology of complex fluids, Oxford University Press, New York, 1999.
[42] G.A. McConnell, M.Y. Lin, A.P. Gast, Long range order in polymeric micelles under steady shear, Macromolecules 28 (1995) 6754–6764, https://doi.org/10.1021/ma00124a009.